Protein Glycosylation

International Edition: DOI: 10.1002/anie.201807054
German Edition: DOI: 10.1002/ange.201807054

A Hierarchical Coding Strategy for Live Cell Imaging of Protein-Specific Glycoform

Siqiao Li, Yiran Liu, Lu Liu, Yimei Feng, Lin Ding, and Huangxian Ju**

Abstract: *Live cell imaging of protein-specific glycoforms holds great promise for revolutionizing the study of glycochemistry. The imaging protocols developed thus far build upon the paired interplay of probe units, thus limiting the number of monosaccharide identification channels. A hierarchical coding (HieCo) imaging strategy, with DNA coding and decoding of protein and monosaccharides executed in fidelity to the hierarchical order of target glycoprotein, is reported herein and features expandable monosaccharide identification channels. A proof-of-concept protocol has been developed for MUC1-specific imaging of terminal sialic acid (Sia) and fucose (Fuc) on MCF-7, T47D, MDA-MB-231, and PANC-1 cells, revealing distinct monosaccharide patterns for four types of cells. The protocol also permits dynamic monitoring of changes in MUC1-specific monosaccharide patterns associated with both the alteration of cellular physiological states and the occurrence of a biologically important process.*

Hierarchy is a ubiquitous structural feature used by living systems to achieve functional diversity.[1,2] DNA,[1a] RNA,[1b] and proteins[1c] can all have characteristic, extrinsic, single- or multi-level appendage structures emanating from the respective core structures. In these branching-type hierarchical structures, the appendage structures serve as a critical handle for regulating the functions of core structures. In particular, protein glycosylation is a post-translational modification that showcases the quintessence of diversity and complexity emergence in structural and functional spaces.[1c] The glycosylation pattern associated with a protein, or glycoform, as characterized by the collection of appended monosaccharides and corresponding linkages in the form of glycans, is under elaborate cellular synthetic control and plays a dictating role in defining the trafficking and signaling properties of the protein and residing cells.[3,4] Live cell imaging of protein-specific glycoforms can therefore not only offer insight into glycosylation pathways and functions but also contribute to the identification of diagnostic and therapeutic targets.[5]

Current protein-specific glycoform imaging strategies rely exclusively on complementary physical (Förster resonance energy transfer)[6a–e] or chemical (proximity catalysis)[6f] interplay of two partner probe units, located, respectively, at the protein and carbohydrate sites of interest, for the intra-glycoprotein-confined generation of readout signals. Despite the effectiveness, the pairing nature of the imaging architecture inherently embedded in these approaches does not mirror the authentic hierarchical structure of a glycoprotein and, as such, will inevitably limit the number of available signaling channels.

An ideal imaging method should allow, in principle, decodable encoding of an arbitrarily expandable number of structural motifs in a glycoprotein with distinct identification codes to fully track its dynamic structural status. With this ideal trait in mind, we report herein the development of a hierarchical coding (HieCo) strategy for live cell imaging of protein-specific glycoform (Scheme 1). The HieCo imaging architecture encodes and decodes each structural motif of interest in a multilevel intra-glycoprotein hierarchical order in fidelity to the target glycoprotein, thus enabling the arbitrary expansion of signaling channels. Specifically, as a prototype demonstration, the coding hierarchy, in higher to lower level order, starts with timing coding, followed by

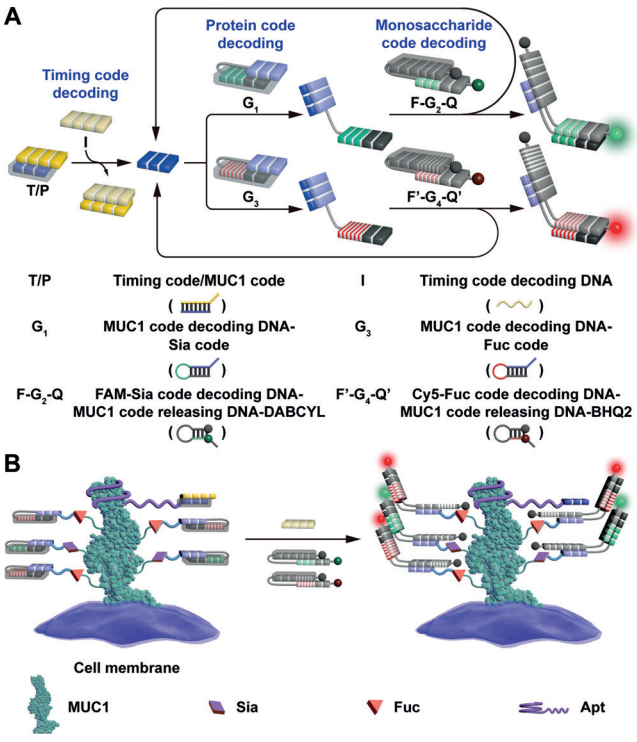

Scheme 1. The hierarchical coding (HieCo) strategy (A) for live cell imaging of protein-specific glycoform (B).

[*] S. Li, Y. Liu, L. Liu, Y. Feng, Prof. Dr. L. Ding, Prof. Dr. H. Ju
State Key Laboratory of Analytical Chemistry for Life Science
School of Chemistry and Chemical Engineering
Nanjing University, Nanjing 210023 (China)
E-mail: dinglin@nju.edu.cn
hxju@nju.edu.cn

Supporting information and the ORCID identification number(s) for the author(s) of this article can be found under: https://doi.org/10.1002/anie.201807054.

protein coding, and ends with monosaccharide coding (Scheme 1 A). The protein and monosaccharide codes are initially concealed in the masked state, and the decoding process commences with the timing code and proceeds in a sequential, iterative decoding–unmasking, catalytic fashion: each decoding of a higher level code leads to the unmasking and exposure of the immediately lower level code for the next round of decoding, except for the final step in each catalytic cycle; the final decoding of monosaccharide code completes the catalytic cycle by simultaneous provision of readout signal and release of protein code. The introduction of timing code allows the stringent temporal separation of coding and decoding processes as well as the initiation of the imaging event at any desired time point. The catalytic utility of the protein code ensures the objective decoding of multiple monosaccharide codes in a fashion reflecting the genuine abundance of each monosaccharide.

For the proof-of-concept demonstration, MUC1-bound terminal sialic acid (Sia) and fucose (Fuc) are selected as the imaging targets.[4,7,8] For the implementation of the HieCo imaging architecture, a unique DNA sequence is created as an identification code each for timing, MUC1, Sia, and Fuc (Scheme 1 B). The timing code (**T**) contains two segments, with one segment partially complementary to the MUC1 code (**P**) and the other segment as a toehold at the 5′ end (refer to Table S1 for DNA sequence information). **P** is connected to an extracellular MUC1-binding aptamer (Apt) S2.2[9] to generate a MUC1-targeting sequence **P**-Apt. The hybridization of **T** with **P**-Apt enables the binding of double-stranded **T**/**P**-Apt to MUC1, with **P** in the masked state and incapable of being decoded through DNA hybridization. The Sia code is connected to a **P** decoding DNA sequence to form a hairpin structure ($\mathbf{G_1}$): the Sia code is caged in the masked state; **P** decoding DNA carries a toehold segment at the 5′ end. $\mathbf{G_1}$ is covalently attached to Sia through the metabolic engineering introduction of an azide group onto Sia followed by a bioorthogonal Cu^I-free click reaction with the 5′-end dibenzocyclooctyne (DBCO)-modified $\mathbf{G_1}$ (DBCO-$\mathbf{G_1}$).[10] Similarly, the hairpin $\mathbf{G_3}$ (masked Fuc code connected to **P** decoding DNA) is covalently linked to Fuc through a Cu^I-catalyzed click reaction between a metabolically engineered alkyne group on Fuc and a 5′-end azide group on $\mathbf{G_3}$ (as N_3-$\mathbf{G_3}$).[10] The decoding process is divided into three stages (Scheme 1). The first stage is the initiation of decoding action by hybridizing a **T** decoding DNA sequence (**I**) with **T** (via toehold-mediated strand displacement[11]), resulting in the simultaneous release and unmasking of **P**. The second stage ensues by intra-MUC1 proximity decoding of **P** with $\mathbf{G_1}$, and via the opening of hairpin structure, unmasking of Sia code (or with $\mathbf{G_3}$ and unmasking of Fuc code). For the third stage, a hairpin structure with both decoding and signal-generating capabilities is required: connection of a 5′-end toehold-bearing Sia code (or Fuc code) decoding DNA sequence with a DNA sequence capable of displacing **P**, together with the installation of a fluorophore near the 5′ end (FAM for Sia code, or F; Cy5 for Fuc code, or F′) and a quencher at the 3′ end (DABCYL for Sia code, or Q; BHQ2 for Fuc code, or Q′), yields either F-$\mathbf{G_2}$-Q or F′-$\mathbf{G_4}$-Q′. The decoding of Sia code on $\mathbf{G_1}$ with F-$\mathbf{G_2}$-Q (or Fuc code on $\mathbf{G_3}$ with F′-$\mathbf{G_4}$-Q′) provides a hairpin opening-derived fluorescence signal and releases **P** for the next catalytic cycle. A recent important finding of artificial cysteine glycosylation by the Chen group raises a caveat on the use of the metabolic engineering approach.[12] In the case of MUC1, the three cysteines are located on the C-terminal, intracellular region, and thus do not interfere with the extracellular HieCo imaging process.

With all the coding and decoding sequences designed, we proceeded to the in vitro validation of the working principle of hierarchical decoding. A key factor in determining the effectiveness of the hierarchical decoding process is the masking efficacy of **T** for **P** (inhibition of background signal) and the decoding–initiating efficacy of **I** (production of readout signal). Optimization reveals a highest hierarchical decoding efficiency, as reflected in the fluorescence intensity (FI), for a **T** variant (used hereafter, Figure S1). The positioning of F and Q at $\mathbf{G_1}$ (or F′ and Q′ at $\mathbf{G_3}$) offers an avenue to compare the readout signal stalled at the stoichiometric $\mathbf{G_1}$ (or $\mathbf{G_3}$) decoding stage with that after the execution of the $\mathbf{G_2}$ (or $\mathbf{G_4}$) decoding catalytic cycle. Indeed, the FI exhibits a low value for a system of **P**-Apt, F-$\mathbf{G_1}$-Q (or F′-$\mathbf{G_3}$-Q′) but increases significantly with the participation of $\mathbf{G_2}$ (or $\mathbf{G_4}$), verifying the ability to achieve catalytic turnover (Figure S2). Important prerequisites for the orderly execution of each hierarchical decoding step are that 1) **T** constrains **P** tightly in the masked state unless being acted upon by **I**, 2) **I** cannot skip the **T** decoding and directly proceed to the unmasking of Sia code and Fuc code, and 3) $\mathbf{G_2}$ and $\mathbf{G_4}$ are not capable of directly accomplishing the respective decoding of masked-state Sia code and Fuc code. Failure to meet these prerequisites will cause the loss of protein identity information and deliver false-positive signals. To rule out these undesired interfering reactivities, twelve systems were examined. Indeed, compared to the intended high FI from systems of both **I**, **T**/**P**-Apt, F-$\mathbf{G_1}$-Q, $\mathbf{G_2}$ and **I**, **T**/**P**-Apt, F′-$\mathbf{G_3}$-Q′, $\mathbf{G_4}$, all ten control systems (without **I** and/or **T**/**P**-Apt) display a background-level signal (Figures S2 and S3).

With all the catalytic hierarchical decoding features unambiguously validated, we next replaced the two components from the decoding system, F-$\mathbf{G_1}$-Q and $\mathbf{G_2}$ (or F′-$\mathbf{G_3}$-Q′ and $\mathbf{G_4}$), with $\mathbf{G_1}$ and F-$\mathbf{G_2}$-Q (or $\mathbf{G_3}$ and F′-$\mathbf{G_4}$-Q′), as used in the live cell protein-specific glycoform imaging setting. The FI shows an analogously pronounced increase only upon the catalytic completion of all hierarchical decoding steps (Figures S4 and 1 A,B). Also, native polyacrylamide gel electrophoresis (PAGE) analysis on a system of **I**, **T**/**P**-Apt, $\mathbf{G_1}$ (or $\mathbf{G_3}$), $\mathbf{G_2}$ (or $\mathbf{G_4}$) identifies a prominent $\mathbf{G_1}$/$\mathbf{G_2}$ (or $\mathbf{G_3}$/$\mathbf{G_4}$) band (Figures S4 and 1 C,D). The simultaneous imaging of two protein-bound monosaccharides requires the elimination of cross-interference between two decoding systems, $\mathbf{G_1}$, $\mathbf{G_2}$, and $\mathbf{G_3}$, $\mathbf{G_4}$. Both FI measurement on F-$\mathbf{G_1}$-Q, F-$\mathbf{G_2}$-Q, $\mathbf{G_3}$, $\mathbf{G_4}$ (no formation of F-$\mathbf{G_1}$-Q/$\mathbf{G_3}$, F-$\mathbf{G_1}$-Q/$\mathbf{G_4}$, F-$\mathbf{G_2}$-Q/$\mathbf{G_3}$, and F-$\mathbf{G_2}$-Q/$\mathbf{G_4}$, Figure S5) and PAGE analysis on **P**-Apt, $\mathbf{G_1}$, $\mathbf{G_2}$, $\mathbf{G_3}$, $\mathbf{G_4}$ (no $\mathbf{G_1}$/$\mathbf{G_3}$, $\mathbf{G_1}$/$\mathbf{G_4}$, $\mathbf{G_2}$/$\mathbf{G_3}$, and $\mathbf{G_2}$/$\mathbf{G_4}$ bands, Figure 1 E,F) corroborate the restriction of decoding action within each intended pair.

With the fundamental working principle of hierarchical decoding demonstrated in vitro, we next examined its utility in the live cell imaging of protein-specific glycoform. The

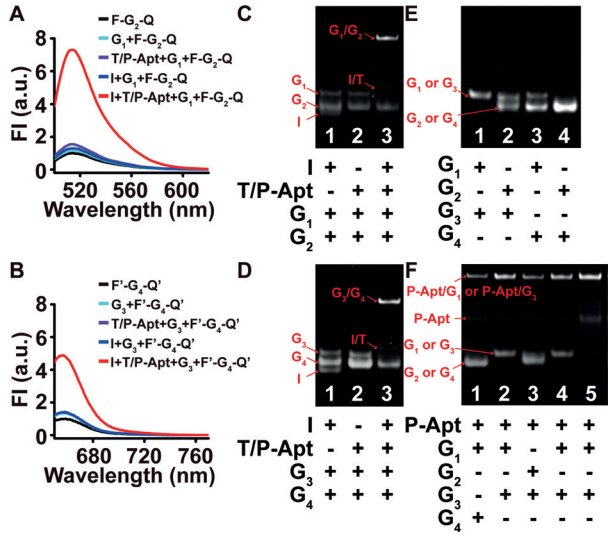

Figure 1. In vitro validation of the working principle of the HieCo strategy. Fluorescence analysis of systems of **I**, **T**/**P**-Apt, $\mathbf{G_1}$, F-$\mathbf{G_2}$-Q (A) and **I**, **T**/**P**-Apt, $\mathbf{G_3}$, F′-$\mathbf{G_4}$-Q′ (B). The 518 nm peak FI for F-$\mathbf{G_2}$-Q (A) and F′-$\mathbf{G_4}$-Q′ (B) is set to 1. Native PAGE analysis of systems of **I**, **T**/**P**-Apt, $\mathbf{G_1}$, $\mathbf{G_2}$ (C) and **I**, **T**/**P**-Apt, $\mathbf{G_3}$, $\mathbf{G_4}$ (D). Native PAGE analysis of a system of $\mathbf{G_1}$, $\mathbf{G_2}$, $\mathbf{G_3}$, $\mathbf{G_4}$ in the absence (E) and presence (F) of **P**-Apt. Lanes 1–4 of (F): incubation of **P**-Apt with $\mathbf{G_1}$ and then with $\mathbf{G_4}$ (1) or $\mathbf{G_3}$ (2), or with $\mathbf{G_3}$ and then with $\mathbf{G_2}$ (3) or $\mathbf{G_1}$ (4). Lane 5 of (F): incubation of **P**-Apt, respectively with $\mathbf{G_1}$ and $\mathbf{G_3}$, and then mixing of the two solutions. Refer to Figures S3–S5 for details.

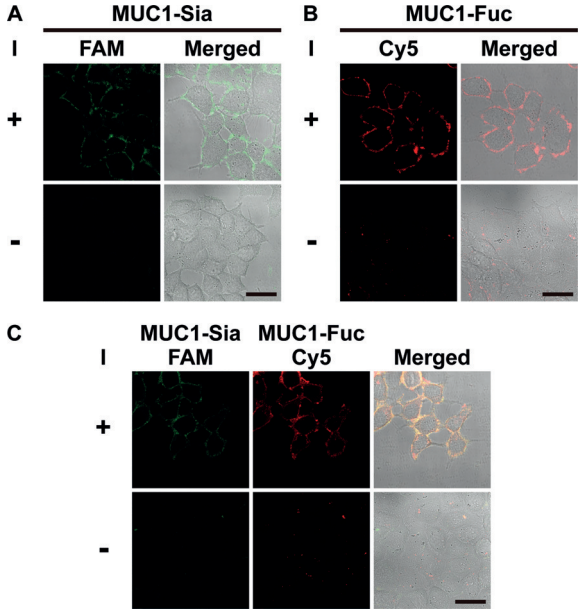

Figure 2. HieCo imaging of MUC1-bound terminal Sia and Fuc on MCF-7 cells. HieCo single-channel imaging of MUC1-bound terminal Sia (A) and Fuc (B) and duplexed imaging in both channels (C). Scale bars: 25 μm.

MUC1-binding affinity of Apt, in the form of either **P**-Apt or **T**/**P**-Apt, is retained,[13] as evidenced under confocal laser scanning microscopy (CLSM) imaging, by the observation of bright fluorescence on MUC1-positive MCF-7 cells[14] and the lack of fluorescence on MUC1-negative HepG2 cells[14] upon incubation in either FAM-**P**-Apt or **T**/FAM-**P**-Apt (Figure S6). As expected, without Apt, **T** alone (as **T**-FAM) is not capable of binding to MCF-7 cells (Figure S7). The Apt sequence requirement for MUC1 targeting is echoed in the loss of binding affinity for a random-sequenced DNA (Ran) (as FAM-**P**-Ran) (Figure S6). No endocytosis is identified for **T** and **T**/**P**-Apt, as examined with FAM-**P**-Apt and **T**-FAM/**P**-Apt (Figure S7); **P**-Apt bound on the MCF-7 cell surface maintains the hybridization capability toward **T** (as **T**-FAM) (Figure S7). The metabolic engineering incorporation of azide-modified Sia and alkyne-modified Fuc[10] allows routine covalent conjugation of DBCO-$\mathbf{G_1}$ and N_3-$\mathbf{G_3}$, respectively, as verified by CLSM imaging of the click reaction with DBCO-FAM-$\mathbf{G_1}$ and N_3-$\mathbf{G_3}$-Cy3 (Figure S8).

With hierarchical decoding probe units, MUC1-docked **T**/**P**-Apt and Sia-linked $\mathbf{G_1}$, installed in place, live cell imaging of MUC1-bound terminal Sia can be achieved (Figure 2A). Indeed, **I** and F-$\mathbf{G_2}$-Q allow the execution of hierarchical decoding with **T**/**P**-Apt and $\mathbf{G_1}$ units. No hierarchical decoding occurs with either the omission of **I** (Figure 2A) or the replacement of F-$\mathbf{G_2}$-Q by F′-$\mathbf{G_4}$-Q′ (Figure S8). The catalytic nature of the hierarchical decoding is validated by the observation of a pronounced increase in FI on MCF-7 cells with $\mathbf{G_2}$ engaged in the decoding hierarchy for **I**, **T**/**P**-Apt, Sia-linked F-$\mathbf{G_1}$-Q (Figure S9). Live cell imaging of MUC1-bound terminal Fuc can be analogously performed by the hierarchical decoding with **I**, F′-$\mathbf{G_4}$-Q′, MUC1-docked **T**/**P**-Apt, Fuc-linked $\mathbf{G_3}$ (Figure 2B). Again, **I** is essential to the decoding process (Figure 2B) and no cross-interference from F-$\mathbf{G_2}$-Q is observed (Figure S8). The simultaneous incorporation of MUC1-docked **T**/**P**-Apt, Sia-linked $\mathbf{G_1}$, and Fuc-linked $\mathbf{G_3}$ (Figure S8) enables duplexed imaging of MUC1-bound terminal Sia and Fuc on MCF-7 cells by decoding with **I**, F-$\mathbf{G_2}$-Q, F′-$\mathbf{G_4}$-Q′ (Figure 2C). The Sia and Fuc imaging channel FI can provide a quantitative measure of their apparent relative abundance. The heterogeneity in the FI distribution around cell contours reflects both heterogeneity in the distribution of MUC1-bound terminal Sia and Fuc and heterogeneity in the cell population, as also confirmed by immunofluorescence imaging of MUC1 (Figure S10).

The confinement of imaging targets as MUC1-bound terminal Sia and Fuc is demonstrated with three sets of experiments. MUC1 is an *O*-glycosylated protein[7] and consistent with this, treatment of MCF-7 cells with benzyl 2-acetamido-2-deoxy-α-D-galactopyranoside (BAG, an *O*-glycosylation inhibitor)[15a] but not with tunicamycin (TM, an *N*-glycosylation inhibitor)[15b] significantly diminishes the imaging FI for both Sia and Fuc (Figures S11 and 3A,B). In further support of MUC1 imaging specificity, up-regulation and down-regulation of MUC1 expression level (Figure S12), respectively with M-pcDNA and shRNA plasmids (Schemes S1 and S2),[16] result in the corresponding increase and decrease of FI (Figures S13 and 3C–F). The terminal Sia and Fuc imaging specificity is verified by the reduction of the FI of the corresponding imaging channel upon the trimming of Sia with α2-3,6,8,9 neuraminidase A (NEU)[17a] and the trimming of Fuc with α-L-fucosidase (AFU)[17b] (Figures S14 and 3G,H). Taken together, the protein and monosaccharide specificity verification experiments also demonstrate the

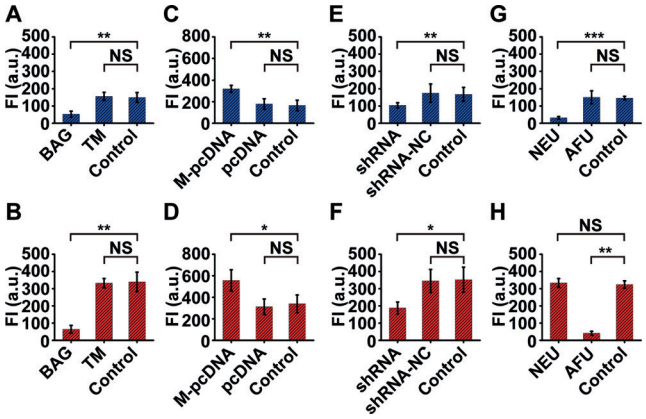

Figure 3. Demonstration of MUC1-bound terminal Sia and Fuc as the imaging targets. HieCo imaging showing the decrease of FI under BAG but not TM treatment (A, B), the increase and decrease of FI with the respective transfection of M-pcDNA (C, D, pcDNA as a control plasmid) and shRNA (E, F, shRNA-NC as a control plasmid), decrease of FI in Sia imaging channel under NEU treatment (G) and decrease of FI in Fuc imaging channel under AFU treatment (H). Blue bars: FI in Sia imaging channel. Red bars: FI in Fuc imaging channel. Statistical analysis: t-test (*$p < 0.05$; **$p < 0.01$; ***$p < 0.001$; NS, not significant).

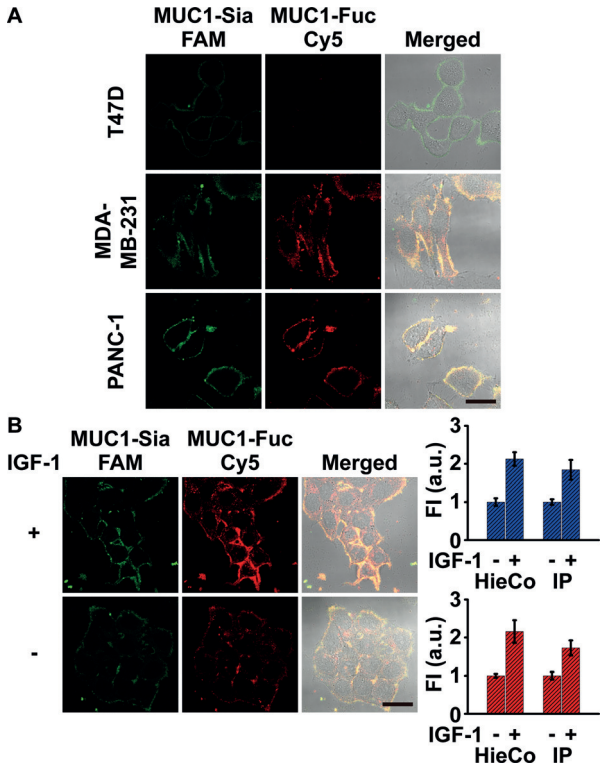

Figure 4. Demonstration of the versatile applicability of HieCo strategy. A) HieCo imaging of MUC1-bound terminal Sia and Fuc on T47D, MDA-MB-231, and PANC-1 cells. B) HieCo imaging as an effective tool for monitoring the EMT process (left). Increase of FI in both of the MUC1-bound terminal Sia (top right) and Fuc (bottom right) imaging channels and confirmation with IP fluorescence analysis. The FI before EMT is set to 1. Scale bars: 25 μm.

ability to dynamically monitor protein-specific glycoform changes with the alteration of cellular physiological states. Systematic HieCo imaging reveals detection limits of 9300 MUC1/cell (via Sia channel) and 10400 MUC1/cell (via Fuc channel) for MUC1 (Figure S15),[18] 7.90×10^5 MUC1-bound terminal Sia/cell for Sia, and 1.08×10^6 MUC1-bound terminal Fuc/cell for Fuc (Figure S16), respectively.

The HieCo strategy can be extended equally effectively to the imaging of MUC1-bound terminal Sia and Fuc on other types of cells, including T47D,[19a] MDA-MB-231,[19b] and PANC-1 cells[19c] (Figures S17 and 4A). The relative abundance of MUC1-bound terminal Sia and Fuc shows a distinct pattern for each cell type (1:1.8, 1:0.6, 1:2.0, 1:1.1 for MCF-7, T47D, MDA-MB-231, PANC-1 cells, respectively).[20] In addition, the HieCo strategy can also be used for identifying the occurrence of a biological process. The epithelial-to-mesenchymal transition (EMT) is an important cellular event featuring the loss of epithelial cells' polarity and adhesion and acquisition of mesenchymal cells' motility and invasiveness.[21a] Associated with the induction of EMT (by insulin-like growth factor 1, or IGF-1) (Figure S18),[21b,c] HieCo imaging reveals an increase of FI for both of the MUC1-bound terminal Sia and Fuc imaging channels (Figures 4B, S18, and S19),[21d] enabling its use as an effective EMT monitoring tool. This observation is also supported by immunoprecipitation (IP) fluorescence analysis (Figure 4B).

In summary, a HieCo strategy has been developed for live cell imaging of protein-specific glycoform. The hierarchical DNA coding architecture established in fidelity to the hierarchical structural order of target glycoprotein permits confinement of hierarchical decoding process in an intra-glycoprotein manner. The successful imaging of MUC1-bound terminal Sia and Fuc on MCF-7, T47D, MDA-MB-231, and PANC-1 cells and the dynamic monitoring capability demonstrate the versatile applicability of the strategy. Given the virtually unlimited choice of DNA coding sequences and decoding pathways, the HieCo strategy should enable comprehensive profiling of monosaccharides of diverse structural types and hierarchical levels and therefore facilitate a more thorough understanding of protein glycosylation processes.

Acknowledgements

We gratefully acknowledge support from the National Natural Science Foundation of China (21675082, 21635005) and the National Basic Research Program of China (2014CB744501).

Conflict of interest

The authors declare no conflict of interest.

Keywords: DNA · glycosylation · live cell imaging · metabolic engineering · protein-specific glycoform

How to cite: *Angew. Chem. Int. Ed.* **2018**, *57*, 12007–12011
Angew. Chem. **2018**, *130*, 12183–12187

[1] a) C. D. Allis, T. Jenuwein, *Nat. Rev. Genet.* **2016**, *17*, 487 – 500; b) B. S. Zhao, I. A. Roundtree, C. He, *Nat. Rev. Mol. Cell Biol.* **2017**, *18*, 31 – 42; c) K. K. Palaniappan, C. R. Bertozzi, *Chem. Rev.* **2016**, *116*, 14277 – 14306.
[2] Y. Lu, A. A. Aimetti, R, Langer, Z. Gu, *Nat. Rev. Mater.* **2017**, *2*, 16075.
[3] F. Bard, J. Chia, *Trends Cell Biol.* **2016**, *26*, 379 – 388.
[4] S. R. Stowell, T. Ju, R. D. Cummings, *Annu. Rev. Pathol.* **2015**, *10*, 473 – 510.
[5] B. Ovryn, J. Li, S. L. Hong, P. Wu, *Curr. Opin. Chem. Biol.* **2017**, *39*, 39 – 45.
[6] a) Y. Haga, K. Ishii, K. Hibino, Y. Sako, Y. Ito, N. Taniguchi, T. Suzuki, *Nat. Commun.* **2012**, *3*, 907; b) B. Belardi, A. de la Zerda, D. R. Spiciarich, S. L. Maund, D. M. Peehl, C. R. Bertozzi, *Angew. Chem. Int. Ed.* **2013**, *52*, 14045 – 14049; *Angew. Chem.* **2013**, *125*, 14295 – 14299; c) W. Lin, Y. Du, Y. Zhu, X. Chen, *J. Am. Chem. Soc.* **2014**, *136*, 679 – 687; d) F. Doll, A. Buntz, A.-K. Späte, V. F. Schart, A. Timper, W. Schrimpf, C. R. Hauck, A. Zumbusch, V. Wittmann, *Angew. Chem. Int. Ed.* **2016**, *55*, 2262 – 2266; *Angew. Chem.* **2016**, *128*, 2303 – 2308; e) N. Wu, L. Bao, L. Ding, H. Ju, *Angew. Chem. Int. Ed.* **2016**, *55*, 5220 – 5224; *Angew. Chem.* **2016**, *128*, 5306 – 5310; f) J. Hui, L. Bao, S. Li, Y. Zhang, Y. Feng, L. Ding, H. Ju, *Angew. Chem. Int. Ed.* **2017**, *56*, 8139 – 8143; *Angew. Chem.* **2017**, *129*, 8251 – 8255.
[7] N. Martínez-Sáez, J. M. Peregrina, F. Corzana, *Chem. Soc. Rev.* **2017**, *46*, 7154 – 7175.
[8] a) O. M. T. Pearce, H. Laeubli, *Glycobiology* **2016**, *26*, 111 – 128; b) M. Schneider, E. Al-Shareffi, R. S. Haltiwanger, *Glycobiology* **2017**, *27*, 601 – 618.
[9] C. S. M. Ferreira, C. S. Matthews, S. Missailidis, *Tumor Biol.* **2006**, *27*, 289 – 301.
[10] L. Feng et al., *J. Am. Chem. Soc.* **2013**, *135*, 9244 – 9247.
[11] Y. Zhao, F. Chen, Q. Li, L. Wang, C. Fan, *Chem. Rev.* **2015**, *115*, 12491 – 12545.
[12] W. Qin et al., *Angew. Chem. Int. Ed.* **2018**, *57*, 1817 – 1820; *Angew. Chem.* **2018**, *130*, 1835 – 1838.
[13] J. Zhou, J. Rossi, *Nat. Rev. Drug Discovery* **2017**, *16*, 181 – 202.
[14] C. Yu, Y. Hu, J. Duan, W. Yuan, C. Wang, H. Xu, X.-D. Yang, *Plos One* **2011**, *6*, e24077.
[15] a) A. Paszkiewicz-Gadek, H. Porowska, D. Lemancewicz, S. Wolczynski, A. Gindzienski, *Int. J. Mol. Med.* **2006**, *17*, 669 – 674; b) L. Zhang, M. Gallup, L. Zlock, Y. T. F. Chen, W. E. Finkbeiner, N. A. McNamara, *J. Pathol.* **2014**, *234*, 60 – 73.
[16] Z. Yuan, S. Wong, A. Borrelli, M. A. Chung, *Biochem. Biophys. Res. Commun.* **2007**, *362*, 740 – 746.
[17] a) Y. H. Li, X. Chen, *Appl. Microbiol. Biotechnol.* **2012**, *94*, 887 – 905; b) Z. Tu, Y.-N. Lin, C.-H. Lin, *Chem. Soc. Rev.* **2013**, *42*, 4459 – 4475.
[18] T. Gao, B. Wang, L. Shi, X. Zhu, Y. Xiang, J. Anzai, G. Li, *Anal. Chem.* **2017**, *89*, 10776 – 10782.
[19] a) R. Beatson et al., *Nat. Immunol.* **2016**, *17*, 1273 – 1281; b) R. Kaukonen et al., *Nat. Commun.* **2016**, *7*, 12237; c) S. J. Jeong, J. H. Kim, B. J. Lim, I. Yoon, J. A. Song, H. S. Moon, D. Kim, D. K. Lee, S. Kim, *Exp. Mol. Med.* **2018**, *50*, e424.
[20] S. Müller, F.-G. Hanisch, *J. Biol. Chem.* **2002**, *277*, 26103 – 26112.
[21] a) I. Pastushenko et al., *Nature* **2018**, *556*, 463 – 468; b) L. A. Walsh, S. Damjanovski, *Cell Commun. Signaling* **2011**, *9*, 10; c) J. Du, S. Hong, L. Dong, B. Cheng, L. Lin, B. Zhao, Y.-G. Chen, X. Chen, *J. Biol. Chem.* **2015**, *290*, 12000 – 12013; d) G. Liao, M. Wang, Y. Ou, Y. Zhao, *Cell. Signalling* **2014**, *26*, 2131 – 2137.

Manuscript received: June 20, 2018
Accepted manuscript online: July 24, 2018
Version of record online: August 8, 2018

